Ocean Science

Modelling the barotropic sea level in the Mediterranean Sea using data assimilation

Marco Bajo[1], **Christian Ferrarin**[1], **Georg Umgiesser**[1,2], **Andrea Bonometto**[3], and **Elisa Coraci**[3]

[1]Institute of Marine Sciences, National Research Council, Castello 2737/F, 30122 Venice, Italy
[2]Klaipėda University, Coastal Research and Planning Institute, H. Manto 84, 92294 Klaipėda, Lithuania
[3]Italian Institute for Environmental Protection and Research, S. Marco, 4665, 30122 Venice, Italy

Correspondence: Marco Bajo (marco.bajo@ve.ismar.cnr.it)

Abstract. This paper analyses the variability of the sea level barotropic components in the Mediterranean Sea and their reproduction using a hydrodynamic model with and without data assimilation. The impact of data assimilation is considered both in reanalysis and short-forecast simulations. We used a two-dimensional finite element model paired with an ensemble Kalman filter, which assimilated hourly sea level data from 50 stations in the Mediterranean basin. The results brought about a significant improvement given by data assimilation in the reanalysis of the astronomical tide, the surge, and the barotropic total sea level, even in coastal areas and far from the assimilated stations (e.g. the southeastern Mediterranean Sea). As with the reanalysis simulations, the forecast simulations, which start from analysis states, improve, especially on the first day (37 % average error reduction) and when seiche oscillations are triggered. Since seiches are free barotropic oscillations that depend only on the initial state, their reproduction improves very effectively with data assimilation. Finally, we estimate the periods and the energy of these oscillations by means of spectral analysis, both in the Adriatic Sea, where they have been extensively studied, and in the Mediterranean Sea, where the present documentation is scarce. While the periods are well reproduced by the model even without data assimilation, their energy shows a good improvement when using it.

1 Introduction

Due to its historical and geopolitical importance, the Mediterranean Sea (Fig. 1) is extensively studied from every point of view, including the physical one. Marine circulation and its main physical, chemical, and biological parameters are the subject of numerous research endeavours at various spatial and temporal scales. With regards to the sea level, the most extreme phenomena, which are caused by meteorological storms in conjunction with astronomical tide (Cavaleri et al., 2019; Ferrarin et al., 2021), happen often in the northern Adriatic Sea (Fig. 1). In the rest of the Mediterranean basin, these phenomena are less frequent, and usually, the sea level variations are studied on a longer timescale linked to the baroclinic circulation. However, even in these parts of the Mediterranean Sea, barotropic variations of the sea level of a few hours and tens to hundreds of kilometres have a certain importance. They can be divided, according to their forcing, into astronomical tide, surges, and seiches (Pugh, 1996).

In the central and northern Adriatic Sea, the shallowness of the continental shelf favours the growth of sea level perturbations. Indeed, the northern Adriatic Sea is one of the Mediterranean regions (as is the Gulf of Gabes) experiencing the highest tidal oscillations (about 1 m at spring tide; Tsimplis et al., 1995). Concerning the surge, the presence of strong autumn southeasterly winds (Scirocco), blowing along the main axis of the basin, favours storm surge events in the north; these are events that can trigger seiche oscillations of considerable intensity (Međugorac et al., 2016). Therefore, the floods in the northern Adriatic coasts, but also in the rest of the Mediterranean coasts, consist of a super-

imposition of astronomical tide, surges, and pre-existing seiches, which are generated by previous storm surge events. In densely populated cities with important cultural heritage, such as Venice and Dubrovnik in the Adriatic or Alexandria in the southeastern Mediterranean basin, it is essential to provide a correct forecast of the sea level at short lead time, from nowcasting up to about 5 d ahead, to alert the population and the authorities of possible flooding events. In this time window, tides, surges, and seiches are the main components influencing the sea level variations. Other possible variations of the sea level related to violent storms could be due to river run-offs, but this component is negligible in the Mediterranean Sea. As asserted before, these phenomena are stronger in the Adriatic Sea, but sometimes the western Mediterranean is subject to strong mistral events (northwesterly winds), and the southern Mediterranean shows the formation of small but intense cyclones with tropical dynamics (called medicanes). These extreme weather conditions have already caused flooding events in the past, even in areas traditionally not affected (Scicchitano et al., 2021).

Regarding the seiches, they are triggered by surge events and have periods determined by the barotropic modes of a basin. While the modes of the Adriatic Sea, being very energetic, have been well studied in the past, those of the Mediterranean Sea are not well known. Although a correct reproduction of seiche oscillations is mandatory in the Adriatic in the case of extreme events, it also improves the sea level under normal conditions in both the Adriatic and the Mediterranean. Furthermore, the investigation of the normal barotropic modes of a basin can also be interesting due to the fact that these modes can be triggered by tsunami waves.

The predictability of tides and surges depends on the predictability of their forcings. The astronomical tide, due to its periodic nature, can be predicted with good accuracy where in situ sea level observations are available. Where these observations are lacking, the tide can be computed by altimeter data (Birol et al., 2017) or by using a hydrodynamic model (with good bathymetry data). With regards to the surge, in the case of severe weather conditions, most of the error on the sea level is due to this part. The surge has a non-periodic nature, depending on the surface wind and atmospheric pressure, and if the meteorological forcing is wrong, the errors can be consistent (Barbariol et al., 2022). Surges can trigger seiches, which propagate for several days, as well as their errors, with different periods and decay times depending on the barotropic modes which they follow. To reduce the errors of these sea level components, data assimilation (DA) procedures can be used. DA aims to reduce the error of the state of a dynamic model at a fixed time by exploiting the available observations of quantities correlated to the model's variables (Kalnay, 2002; Evensen, 2009a; Carrassi et al., 2018). DA can be used to improve the forecast, providing an accurate initial state, which is called the analysis state, and to produce several analysis states to simulate past periods with reduced errors (reanalysis simulation). Usually, the reanaly-

sis simulations are much more accurate than analogous simulations made without the DA (here referred to as hindcast simulations). This is due not only to the assimilation of all the available, well-processed observations but also, if possible, to the use of more accurate forcings and boundary conditions.

The main purpose of this work is to analyse the impact of DA in the reproduction of tides, surges, seiches, and the total sea level made by these components, both in reanalysis and in forecast simulations. With regards to the astronomical tide, the reanalysis simulation can be used to produce more accurate maps of the amphidromic systems of its components. Moreover, harmonic analyses can be executed at each point of the model's grid to determine the amplitudes and phases of the main components in order to obtain forecasts in arbitrary locations. The reanalysis of the surge and the total sea level is useful mainly as a coastal product to produce accurate past climatologies with a good reproduction of extreme events. For example, in the Mediterranean Sea, where the coasts have a large extension compared to the basin's area and where the weather conditions are strongly influenced by the orography, hindcast model simulations without DA often suffer from underestimation errors.

The DA can be used not only for the reanalysis but also for the forecast by improving the initial state of the system. In this work, we use the DA 1 d before each daily forecast to create a final state of analysis from which to start the forecast simulation. The DA improvement is due to the fact that the initial analysis state has a lower error than the one without DA (background state), even if the error coming from the forcing and the boundary condition cannot be corrected. In summary, we run the simulations using a finite-element hydrodynamic model and assimilating, in some of them, data from 50 sea-level coastal stations with an ensemble Kalman filter. The period considered is 2 months long, from the beginning of November to the end of December 2019. In this period, one of the most extreme storm surge events was recorded in Venice, and very energetic seiche oscillations happened some weeks later.

In the following sections, we report the methodology, with a description of the hydrodynamic model (Sect. 2.1), the observation collection and processing (Sect. 2.2), and the DA method and setup (Sect. 2.3). The section ends with a description of all the simulations that we performed (Sect. 2.4). Then we expose the results of the DA calibration (Sect. 3.1), the hindcast and reanalysis simulations (Sect. 3.2), and the forecast simulations (Sect. 3.3). The second part of Sect. 3.3 is dedicated to the description and reproduction in the forecast mode of the November and December 2019 extreme events mentioned before. Finally, the discussion (Sect. 4) and conclusions (Sect. 5) follow.
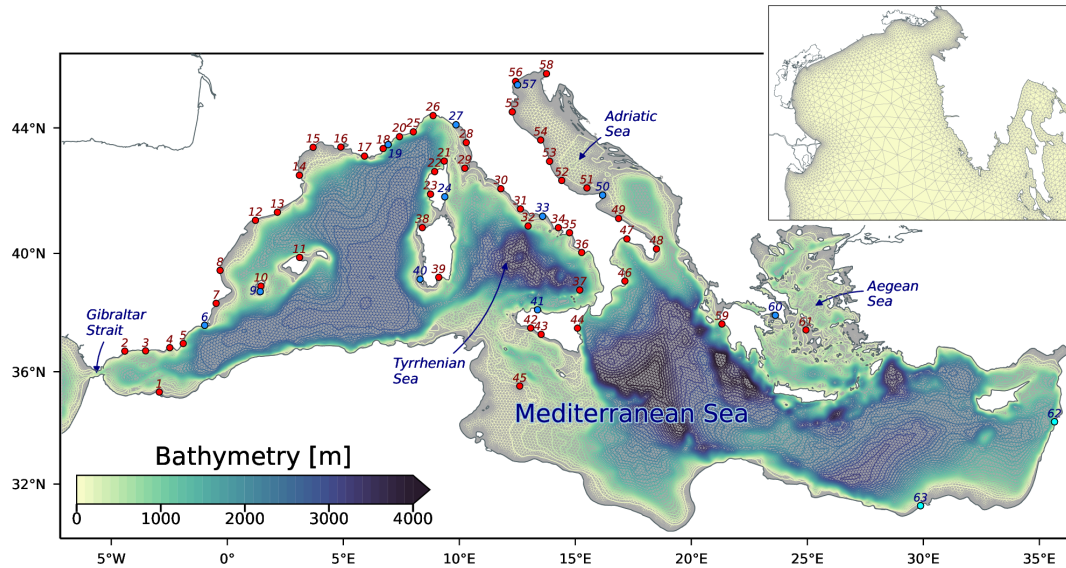
Figure 1. The big panel shows the unstructured grid and the bathymetry used by the model. In the small panel is a zoom of the grid in the northern Adriatic Sea. The red and blue dots mark the locations of the assimilation and validation tide gauges respectively.

2 Methods

2.1 The hydrodynamic model

The hydrodynamic model we use is called SHYFEM (System of HydrodYnamic Finite Element Modules – v7_5_71); it was created at the National Research Council (CNR) in Venice (Umgiesser et al., 2004), where it is largely developed. Its code is available with an open-source license and is freely downloadable from the web (https://github.com/SHYFEM-model/shyfem, last access: 2 May 2023). SHYFEM is composed of a hydrodynamic core that solves the shallow-water equations with the finite-element technique and with a semi-implicit time-stepping algorithm, which allows a remarkable speed of execution. Various terms in the equations can be turned on or off, such as the momentum advection terms, Coriolis terms, baroclinic terms, and tidal potential. The model can be used in two- or three-dimensional modes and allows various formulations of bottom stress and wind stress. Finally, the model can be coupled to various modules or other models (e.g. waves, Lagrangian, ecological).

In this application, we use a two-dimensional barotropic formulation given by the following equations:

$$
\begin{aligned}
\frac{\mathrm{d}U}{\mathrm{d}t} - fV \quad &= \quad -H\left(g\frac{\partial\zeta}{\partial x} + \frac{1}{\rho_{\mathrm{w}}}\frac{\partial p_{\mathrm{a}}}{\partial x}\right), \\
&+ \quad A_{\mathrm{H}}\nabla^2 U + \frac{1}{\rho_{\mathrm{w}}}\left(\tau_{\mathrm{w}x} - \tau_{\mathrm{b}x}\right) \\
\frac{\mathrm{d}V}{\mathrm{d}t} + fU \quad &= \quad -H\left(g\frac{\partial\zeta}{\partial y} + \frac{1}{\rho_{\mathrm{w}}}\frac{\partial p_{\mathrm{a}}}{\partial y}\right), \qquad (1) \\
&+ \quad A_{\mathrm{H}}\nabla^2 V + \frac{1}{\rho_{\mathrm{w}}}\left(\tau_{\mathrm{w}y} - \tau_{\mathrm{b}y}\right) \\
\frac{\partial\zeta}{\partial t} + \frac{\partial U}{\partial x} + \frac{\partial V}{\partial y} \quad &= \quad 0,
\end{aligned}
$$

where the independent variables are the time, t, and where the spatial variables are x and y. $U(x, y, t)$ and $V(x, y, t)$ are the transports along x and y, $f(y)$ is the Coriolis coefficient, and $H(x, y, t)$ is the sum of the sea depth with $\zeta(x, y, t)$, which is the variable level with respect to the resting state; g is the gravitational acceleration, ρ_{w} is the average density of seawater, $p_{\mathrm{a}}(x, y, t)$ is the atmospheric pressure at the sea level, and A_{H} is the horizontal coefficient of turbulent viscosity, formulated with Smagorinsky (1963) using a dimensionless coefficient equal to 0.2; finally, $\nabla^2[\cdot]$ is the two-dimensional Laplacian operator. $\tau_{\mathrm{b}x}(x, y, t)$ and $\tau_{\mathrm{b}x}(x, y, t)$ are the components of the stress at the bottom, expressed with a linear-quadratic formulation with a coefficient equal to 0.0025 (Bajo et al., 2019); $\tau_{\mathrm{w}x}(x, y, t)$ and $\tau_{\mathrm{w}x}(x, y, t)$ are the components of wind stress, expressed with the formulation proposed by Hersbach (2011) and with a Charnock coefficient equal to 0.02. Furthermore, for the simulations that calculate the tidal level or the total sea level, the terms of the tidal potential are also active, and four semi-diurnal (M_2, S_2, N_2, and K_2) and four diurnal components (K_1, O_1, Q_1, and P_1) are calculated.

The model is applied on a mesh of the Mediterranean Sea, which extends into the Atlantic Ocean up to about $7°$ W and has about 163 000 triangular elements. The size of the elements is variable, with a gradually greater resolution from the open sea (element side length of ~ 12 km), to the coasts (element side length of ~ 500 m), as shown in Fig. 1. The bathymetry derives from the 2020 dataset of the European Marine Observation and Data Network (https://www.emodnet-bathymetry.eu/, last access: 2 May 2023), which was bilinearly interpolated on the mesh.

This model has already been used in the past, with similar configurations, in scientific works and is currently used in several operational systems for the sea level prediction. For example, the most extreme storm surge events that occurred in 1966, 2018, and 2019 were studied and simulated in Roland et al. (2009), Cavaleri et al. (2019), and Ferrarin et al. (2021). Various operational versions of the model with similar configurations have been used for over 15 years at the high-tide forecasting and warning centre (CPSM) in Venice (Bajo et al., 2007; Bajo and Umgiesser, 2010; Bajo, 2020) and at the Italian Institute for Environmental Protection and Research (ISPRA – https://www.venezia.isprambiente.it/ispra/modellistica, last access: 2 May 2023). At this institute, a system similar to that described in this paper will be installed in the next months. SHYFEM, with an old DA system, was also used to assess the impact of altimeter data on storm surge forecasting (Bajo et al., 2017) and, using the more recent DA system described in this paper, to study a particular seiche event (Bajo et al., 2019). With regards to the reproduction of the astronomical tide in the Mediterranean and Black seas, a first specific work has been successfully completed (Ferrarin et al., 2018), but a preliminary total-sea-level operational system was set up earlier (Ferrarin et al., 2013). Finally, there are numerous works performed with other hydrodynamic models with barotropic configurations for the study and prediction of tides, surges, seiches, and sea level variations given by these components (see e.g. Flowerdew et al., 2010; Bertin et al., 2014; Fernández-Montblanc et al., 2019; Horsburgh et al., 2021; Byrne et al., 2021).

2.1.1 Surface and lateral boundary conditions and perturbation methods

The simulations use as surface boundary conditions 10 m wind and mean sea level pressure hourly fields provided by the BOLAM atmospheric model (Mariani et al., 2015), which is hydrostatic and runs at an 8 km horizontal resolution. The model is nested in the ECMWF Integrated Forecasting System (IFS – https://www.ecmwf.int/en/publications/ifs-documentation, last access: 2 May 2023). In the hindcast and reanalysis simulations, the surface-forcing fields are made by the first forecast days chained together, while the forecast simulations, which are daily, use the entire forecast up to 5 d ahead.

The lateral boundary conditions are closed everywhere except at the western border in the Atlantic Ocean, near Gibraltar, where the sea level is imposed and where the water transports are left free to adjust (Dirichlet conditions). The open boundary was chosen outside the Mediterranean Sea to reduce the error inside the basin, and different sea level quantities are used depending on the simulation type. For the simulations computing the total sea level, we used the variable sea surface height (SSH) from the Mediterranean Sea Physical Analysis and Forecast system (Clementi et al.,

2021), running at the Copernicus Monitoring Environment Marine Service (CMEMS). For the simulations computing only the surge, we used the de-tided SSH, available in the same dataset, which is the residual part remaining after the harmonic analysis of the SSH. Finally, the simulations computing only the tide use the difference between these two quantities. The SSH and the de-tided SSH can contain a baroclinic part which has lower-frequency variations and cannot be easily filtered out.

In the present work, in which the considered domain is relatively small compared to the speed of the barotropic perturbations, the lateral and surface boundary conditions greatly influence the solution of the equations of motion. Therefore, the physical problem can be defined as more boundary driven than initial-state driven, and the perturbation of the surface and lateral-boundary conditions is necessary to prevent the narrowing of the initial ensemble after a short time. In all the DA simulations, the members of the ensemble are created by perturbing the initial state, and then the spread is maintained by the perturbation of the forcing, the boundary conditions, and some model parameters. The perturbation of the initial state is performed only for the sea level (variable ζ in Eq. 1) with a technique similar to that used for the atmospheric pressure (described later), while the water transports are not perturbed.

In the forecast simulations, the initial state is perturbed only in the first simulation, then the following daily simulations start from the states saved in the previous-day simulations. Even for the reanalysis simulations, the perturbation of the initial state is not very important, as the simulations last for 2 months, and the influence of the forcing and boundary conditions, as well as the assimilated observations, are far more important after some days. Therefore, in reanalysis, the forcing and boundary conditions are perturbed for the entire period of the simulations, while in forecasting, each simulation assimilates observations for 24 h, during which conditions are perturbed, and then 5 d of deterministic forecasting follow, starting from the analysis ensemble mean and using unperturbed forcings and boundary conditions.

The perturbations are calculated so that, for a scalar physical variable, the mean of the perturbed values should be approximately equal to the non-perturbed value and so that the standard deviation should resemble the estimated error; furthermore, the perturbations must belong to a Gaussian distribution. We used this method for the conditions at the lateral open boundary, with the same perturbations in each node. A similar perturbation was also used for the value of the drag coefficient in the bottom stress, with a distribution centred at 0.0025 and with a standard deviation of 0.0005. In the DA simulations using the tidal forcing (tide and total sea level), a calibration factor for the loading tide (parameter "ltidec" in SHYFEM) is perturbed as well, with a mean value of 6×10^{-5} and a standard deviation of 1×10^{-5}.

Perturbing the two-dimensional atmospheric fields is more complex. We still impose the same condition for the mean

and the standard deviation at each point, but the perturbations must have a spatial correlation, and the atmospheric pressure perturbations should be linked to the wind perturbations. We therefore first perturbed the atmospheric pressure field through a technique to generate two-dimensional pseudo-random fields (Evensen, 1994, 2003), imposing a decorrelation length of about 400 km and a standard deviation of 3.5 hPa. These values, slightly different from those used in Sakov et al. (2012), were found empirically, and they produce perturbations at a sub-synoptic scale, with a similar size to the typical Mediterranean cyclones (Ferrarin et al., 2021). From these fields of pressure perturbations, we calculated the corresponding perturbations for the velocity components. If the pressure perturbation in one point is δP, the perturbations for the wind components, in geostrophic equilibrium, are as follows:

$$\delta u = -\frac{\delta P}{\delta y}\frac{1}{\rho_a f},$$
$$\delta v = \frac{\delta P}{\delta x}\frac{1}{\rho_a f}. \tag{2}$$

Using these perturbation fields for application to the unperturbed fields of wind and pressure at an instant t, we obtain perturbed fields with physical coherence. Again for the atmospheric fields, in addition to this kind of perturbation, a temporal perturbation has also been introduced in which, from a field at time t, an ensemble of equal fields is generated but with reference time $t + dt_n$, where dt_n are time perturbations belonging to a Gaussian distribution as well.

Finally, with regards to the perturbations of the forcing and the boundary conditions that vary over time, the error at a given instant t_1 must be correlated to the error at the next instant, t_2. This is defined as red noise and is implemented by calculating a weight dependent on the time interval between the two fields and by defining a decay time as follows:

$$\alpha = 1 - \frac{t_2 - t_1}{\tau}, \tag{3}$$

where τ is the decay time. The perturbation ξ_2 at time t_2 becomes a linear combination of the perturbation ξ_1 at time t_1 and the newly calculated perturbation ξ_2^*:

$$\xi_2 = \alpha \xi_1 + \sqrt{1 - \alpha^2}\xi_2^*. \tag{4}$$

2.2 Observations

2.2.1 In situ data

Sea level observations were retrieved from the European Joint Research Center database (https://data.jrc.ec.europa.eu/, last access: 2 May 2023). As shown in Fig. 1, tide gauges are concentrated in the western and central Mediterranean Sea, mostly along the Spanish, French, and Italian coasts, while on the northern African coast, there is only one station (Melilla), and few stations are present in

the eastern Mediterranean Sea. The Adriatic Sea has stations only along the Italian coast and not on the eastern coast, but they are still quite numerous. The stations in the Mediterranean Sea were divided into 50 stations to be assimilated and 13 stations for the validation (Table A1). The data are recorded every 10 min in the period of October–December 2019. We processed them with the SELENE quality check software (https://puertos-del-estado-medio-fisico.github.io/SELENE/, last access: 2 May 2023 Pérez et al., 2013) for spikes and outliers detection, stability testing, date and time control, flagging, and interpolation of short gaps. Subsequently, the quality-checked data were elaborated with the Python binding of UTide (https://github.com/wesleybowman/UTide, last access: 2 May 2023, http://www.po.gso.uri.edu/~codiga/utide/utide.htm, last access: 2 May 2023) based on the least-squares fitting to separate the tidal periodic part from the non-tidal residual (NTR). We kept the eight most energetic tidal constituents in the harmonic analysis (M_2, S_2, N_2, K_2, K_1, O_1, P_1, and Q_1), which are the most important in the Mediterranean Sea (Ferrarin et al., 2018). The NTR was further processed by applying a 2 h moving average to remove high-frequency signals. The harmonic analysis was not possible for stations 62 and 63 due to the lack of enough continuous data. Therefore, these stations were used only for the validation of the total sea level, for which the harmonic analysis is not necessary.

Finally, the observations from different stations often have different mean sea levels. Sometimes this is due to a different reference datum, which depends on the monitoring network to which they belong. Furthermore, the observed sea level can contain a low-frequency non-barotropic part due to salt and temperature gradients, as well as steric effects. Therefore, we decided to refer all the observations to the 2-month mean sea level computed by a deterministic simulation of the model that we used. A similar approach is adopted in Byrne et al. (2021).

2.2.2 Altimeter data

Altimeter data are difficult to use in storm surge studies, even if some attempts were made in the past (Bajo et al., 2017). Since high-frequency signals are badly sampled by the satellite tracks, this part is usually removed with the help of a barotropic two-dimensional model (Carrère and Lyard, 2003). Normally, in the altimeter products, the tidal part is also removed with a similar barotropic tidal model (Lyard et al., 2021). However, since the altimeters measure the sea level every cycle (about every 10 d) in the same locations, it is possible to extract the tidal part from the signal by means of harmonic analysis.

Recently, the amplitudes and phases of the main harmonic components along the altimeter tracks have become available on the AVISO website (https://doi.org/10.6096/CTOH_X-TRACK_Tidal_2018_01). The X-TRACK along-track tidal constants were computed via harmonic analysis of the sea

level anomalies for long time series missions (Birol et al., 2017). We used the X-TRACK's (based on Topex/Poseidon + Jason-1 + Jason-2) eight most energetic tidal constituents over the Mediterranean Sea (see the list in the previous section) to compute the astronomical tide for the period of our simulations. These data were used in the validation of the tidal reanalysis simulation, as described in Sect. 3.2.

2.3 The data assimilation system

In this section and the following ones, we will use some terminologies and concepts typical of the DA; for an introduction to these concepts and to the different techniques, we recommend reading Carrassi et al. (2018).

The code used for the DA in this paper is based on routines developed and described in Evensen (2003, 2004) and available at https://github.com/geirev/EnKF_analysis, last access: 2 May 2023. These routines have been adapted and extended to be used in the SHYFEM model, allowing for the use of different techniques, such as the ensemble Kalman filter (EnKF) and the ensemble square root filter (EnSRF), and different numerical schemes (https://github.com/marcobj/shyfem, last access: 2 May 2023). Furthermore, various routines have been created to perturb the forcings and boundary conditions in order to obtain ensembles of arbitrary size. In the present work, we used the EnKF with the correction described in Evensen (2004) to avoid the loss of rank in the observation covariance matrix (Kepert, 2004). The system uses the adaptive inflation (Evensen, 2009a) to avoid narrowing of the ensemble spread, and the observations are considered to be independent (they come from different stations). Therefore, the observation covariances are set to zero, while the variances are positive and equal to each other. In order to discard the too-high innovations, a simple technique checks the values of the variances of the background matrices and the observations (Järvinen and Undén, 1997; Storto, 2016).

Finally, to avoid shocks in the model state near the lateral open boundary due to the imposition of the sea level, in the final ensemble states the analysis states are relaxed to the background ones, gradually approaching the boundary. The background and analysis states are weighted through a Gaspari–Cohn (GC) function (Gaspari and Cohn, 1999), prescribing a radius from the nodes of the lateral open boundary. In each node, the model ensemble state after an analysis step is

$$A_a^*(x, y) = A_b(x, y) f(x, y) + (1 - f(x, y)) A_a(x, y), \quad (5)$$

where x and y define the position of the node in the grid, A_b refers to the background states, A_a refers to the analysis states, and f is the GC function, equal to 1 in the open boundary nodes. Since the GC function goes to zero at a distance greater than twice the radius, after this distance, the solution is identical to that of the analysis, while near the boundary, it is similar to the background solution, strongly driven by

the boundary condition and not affected by the analysis increments.

This set of the DA parameters was decided upon after running several calibration tests, some of which are exposed in Sect. 2.4.

2.4 Results' production and post-processing

All the simulations were run in the period from the beginning of November to the end of December 2019. The hindcast and reanalysis simulations are 2 months long with continuous forcing and boundary conditions, as described in Sect. 2.1.1. The reanalysis simulations assimilate the data from the 50 stations every hour throughout the 2 months. From the ensemble states, the analysis ensemble mean is calculated as the best estimate of the real state of the physical system and is used in the examination of the results.

In running the forecast simulations, we used the same settings as those that would be used in an operational context. The period is the same as that considered in the hindcast and reanalysis simulations. However, the simulations are performed daily, and each simulation is composed of a 1 d hindcast (no DA) or analysis (DA) simulation and a 5 d forecast simulation. For the sake of brevity, we will show only the results of the first 3 d. The forecast simulations with DA assimilate the data from the 50 stations every hour in the 24 h preceding the forecast. From the final analysis states, we computed the analysis ensemble mean each day at 00:00 UTC, and we used it as an initial state from which to run the 5 d forecast. Then the analysis states are saved to be used as initial states in the next day's simulation. In this way, the DA always starts from analysis states and is similar to the cycle performed in reanalysis, except for the perturbation of the forcing and boundary conditions, which is made again every day.

To evaluate the results, each daily forecast simulation was divided into five parts, and each part was chained with the corresponding one of the previous and following days. Continuous results are obtained for 1, 2, and 3 d lead times and can be directly compared with the observations. The forecast timeline is shown in Fig. 2 and is the same for the simulations without and with DA.

We calculated the standard deviations of the model and observed data, the correlation between them, and the centred root-mean-squared error (CRMSE). The standard deviations and CRMSEs were normalised to the standard deviation of the observations at each station and were represented by Taylor diagrams (Taylor, 2001). Bias error plots were also calculated, and the bias was calculated as the mean of the differences between the modelled and observed values; the CRMSE represented in the same plots is not normalised. For the sake of clarity, we reported the various simulations in Table 1 with identification labels, which we will use in the following sections.
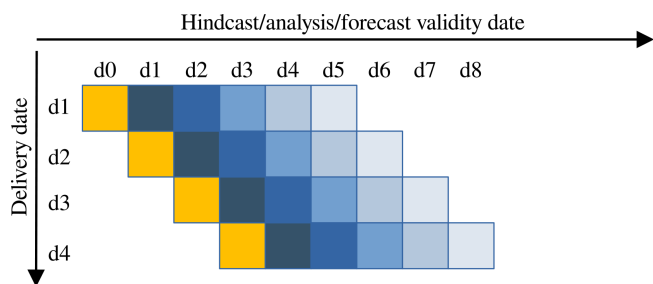
Figure 2. Timeline of the forecast simulations. The squares represent the days, which are expressed as d0, d1, etc. The delivery date is the day when the forecast is supposed to be executed, while the validity date is the length of the forecast. The orange squares are the days of hindcast (without DA) or of analysis (DA). The blue squares are the forecast days, from the first (darkest) to the fifth (lightest).

Table 1. Clusters of simulations executed in this work. The identification label (ID) is composed of the physical variable (T – tide, S – surge, Z – total sea level), by the type of simulation (hindcast, reanalysis, or forecast), and by the use of DA.

ID	Variable	Type	DA
TH	Tide	Hindcast	No
TR_A	Tide	Reanalysis	Yes
SH	Surge	Hindcast	No
SR_A	Surge	Reanalysis	Yes
ZH	Total sea level	Hindcast	No
ZR_A	Total sea level	Reanalysis	Yes
SF	Surge	Forecast	No
SF_A	Surge	Forecast	Yes
ZF	Total sea level	Forecast	No
ZF_A	Total sea level	Forecast	Yes

Regarding the spectral analysis, we used the NTR and the model surge signal in December 2019. The power spectral density was estimated with the Welch method (Welch, 1967), dividing the period into 8 d windows with 50 % overlap. The fast Fourier transform length is rounded up to the nearest integer power of 2 by zero padding.

3 Results

3.1 Calibration of the data assimilation

Before running the final simulations used to produce the results, we carried out numerous experiments to determine the best values of some DA parameters. The parameters that have been varied are the assimilation scheme (EnKF, EnSRF), the error of the observations (we tested from 1 to 3 cm), the radius in Eq. (5), the radius in the domain localisation, and the number of the ensemble members. Although, in fact, the localisation brings advantages in many applications, in our case, the available observations are mainly located in the
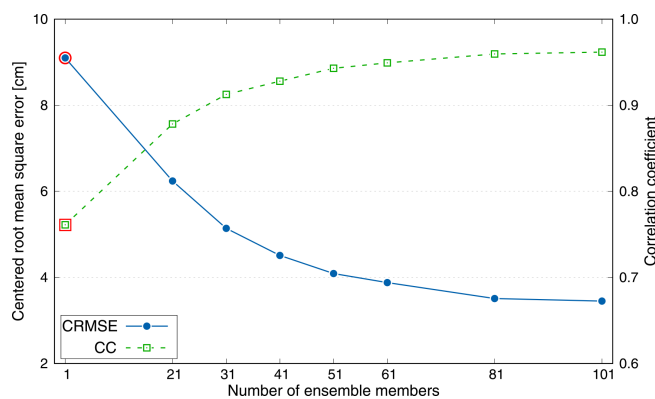

Figure 3. Performance of the data assimilation in terms of CRMSE and correlation coefficient as a function of the number of ensemble members. The red contour highlights the results of the simulation without data assimilation.

northern side of the computational domain. This implies that, to obtain a spatially uniform analysis correction, a large localisation radius should be used to reach the other border of the basin. Furthermore, the correlation radius of a variable (barotropic sea level perturbations, in our case) between a point and its neighbours increases with its propagation speed. In the present case, the propagation speed is that of shallow-water waves (in the western Mediterranean basin, considering an average depth of about 2000 m, the speed is $140\,\mathrm{m\,s}^-$). For these considerations and after having carried out various tests varying the radius of the local analysis, we have decided not to use this method and to increase the number of ensemble members instead. A high number of ensemble members avoids problems of spurious correlations and cross-correlations. Moreover, since the simulations are extremely fast and have a workstation with a high number of cores, the execution time would not affected much. To determine the minimum number of ensemble members to obtain good results without increasing the computational load too much, we performed various total sea level reanalysis simulations. In Fig. 3, we report the centred root-mean-squared error (CRMSE) of the analysis ensemble mean, averaged in the validation stations, using a different number of ensemble members. The error is reduced from 9.3 cm in the case without DA to 3.6 cm using 101 members, and the correlation increases from 0.75 to 0.95. Since the error pattern is regular and asymptotic, we decided to use 81 members.

Therefore, to conclude, the final configuration uses the EnKF with an observation error of 2 cm, a radius in Eq. (5) of 250 km, no localisation techniques, and 81 ensemble members.

3.2 Hindcast and reanalysis simulations

In this section, we analyse the results of the hindcast and reanalysis simulations for the astronomical tide, the surge, and the total sea level. In Fig. 4, the first diagram on the left

shows the astronomical tide comparison, in which the model results without (hindcast) and with (reanalysis) DA are compared with the tide calculated by the harmonic constants (TH, TR_A). The results are good even without DA in almost all stations, with a certain tendency to overestimate the signal amplitude (higher standard deviation). Station 60 is an exception where the results in hindcast are poor, probably due to its position in the Aegean Sea, a morphologically complex area. The results with DA are very good for all the validation stations, reaching almost perfect agreement (correlation of about 0.99), with a small deterioration in station 60, which, however, improves and still achieves a more-than-good accuracy (CRMSE from 4 to 1 cm).

The central diagram shows the reproduction of the surge signal compared with the NTR extracted from the observations (SH, SR_A). In this case, the distribution of the stations in the Taylor diagram is sparse for the deterministic simulation, and station 60 is still the worst. The reanalysis simulation improves considerably the surge reproduction in all the stations, with a very focused distribution, even if it is not like that of the astronomical tide. For example, in station 60, the CRMSE reduced from 8 to 3 cm.

Finally, the simulations with the total sea level (ZH, ZR_A) have a quality similar to that of the surge simulations. Some stations are even better, perhaps thanks to the good accuracy in the reproduction of the tidal signal. As for the surge simulations, the CRMSE goes from 8 cm in the hindcast simulation to 3 cm in the reanalysis.

For the total sea level, we also made a comparison for stations 62 and 63, which, as previously mentioned, are the only ones in the eastern basin and are at least a 1000 km away from the nearest assimilated station. It is interesting to note that these stations demonstrate a consistent improvement; the CRMSE goes from 9.6 to 4 cm for station 62 and from 10.9 to 5.7 cm for station 63. It is probable that this improvement is due to the high number of ensemble members, which allows correct correlations in the background covariance matrix, even for variables that are very distant from each other.

In order to validate the DA even in the open sea, far from the coasts, it is possible to use altimeter data for the computation of the harmonic constants and the tide. The amplitudes and phases of the eight most energetic tidal constants retrieved from the altimetric data were used to calculate the tide oscillations at each point of the satellite tracks in the Mediterranean Sea. To compare this data with the model data, the sea levels from the TH and TR_A simulations were extracted at the same coordinates, and the CRMSE were calculated. Figure 5 shows the along-track differences in the CRMSE (i.e. $CRMSE_{TR_A}$–$CRMSE_{TH}$). The values are negative almost everywhere, clearly showing a marked improvement of the DA in reproducing the tidal levels over the whole basin, with a reduction of the CRMSE up to 20 cm near the Gibraltar Strait, in the Gulf of Gabes, and in the northern Adriatic Sea. It is worth noting that the DA effect is not local, as the areas in which there is a greater improvement do not correspond to-

tally to those with more assimilated stations (e.g. the eastern Mediterranean Sea). Averaging the CRMSE over the whole basin, we obtain a mean value of 11.6 cm for the simulation without DA (TH) and a value of 4.3 cm for the simulation with DA (TR_A).

3.3 Forecast simulations

In this section, we analyse the results of the forecast simulations for the surge component and for the total sea level. In Fig. 6, the Taylor diagrams show the comparison with the observations for the first, second, and third forecast days, both for the model data without DA, starting from a background state, and for those with DA, starting from the analysis ensemble mean. In the results relative to the surge simulations (SF, SF_A), the effect of the DA on the first forecast day is evident, and the distributions are similar to, although slightly worse than, that obtained in the hindcast and reanalysis simulations in Fig. 4 (central panel) The data improves for each validation station, including for station 60, which is far from the nearest assimilated station. Unfortunately, the data in stations 61 and 62 cannot be used in the validation of the surge simulations, as it was not possible to perform the harmonic analysis necessary to subtract the tide due to the scarcity of available data.

The improvement is smaller on the second-day forecast, while on the third day it is almost nil, worsening slightly for some stations. This behaviour is due to the fact that the initial state of the system, as well as its error correction, gradually lose their importance as the forecast moves away from the initial state. The forecast without DA has a larger error in the initial state, which is most prominent on the first and second days of forecasting.

In Fig. 7, we show the bias error for the surge simulations. This plot was not made for the hindcast and reanalysis simulations for which the bias is almost null. The figure shows that the DA improves the results, especially on the first forecast day, following which the correction is still positive but weaker on the second day, while on the third day, the DA slightly worsens the original forecast, in agreement with what has been seen in the Taylor diagrams. The worsening is contained and relates to the third forecast day, which, in an operational context, is of secondary importance compared to the first and second days. Still, observing Fig. 7, it can be seen how station 57 deviates from the others, with a much greater bias and CRMSE. This is due to the position of this station in the northern Adriatic, where the surge signals and the associated seiche oscillations are larger than in the rest of the Mediterranean Sea. However, precisely for this reason and since there are numerous good-quality stations in the Adriatic Sea, the effect of DA is strong in the correction of both random and systematic errors. The systematic errors, represented by the biases in Fig. 7, are almost all positive, denoting an overestimation of the model. This behaviour is true
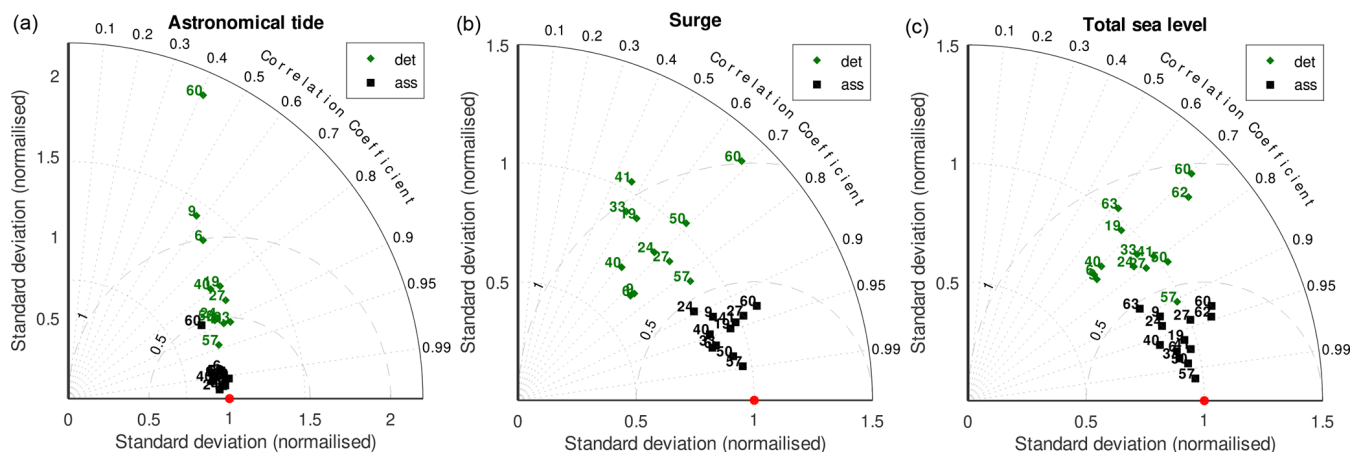
Figure 4. Normalised Taylor diagrams of the hindcast and reanalysis simulations. The deterministic simulations (green diamonds) compared to DA simulations (black squares) for the astronomical tide (**a**), the surge (**b**), and the total sea level (**c**). The red dot indicates the perfect agreement.
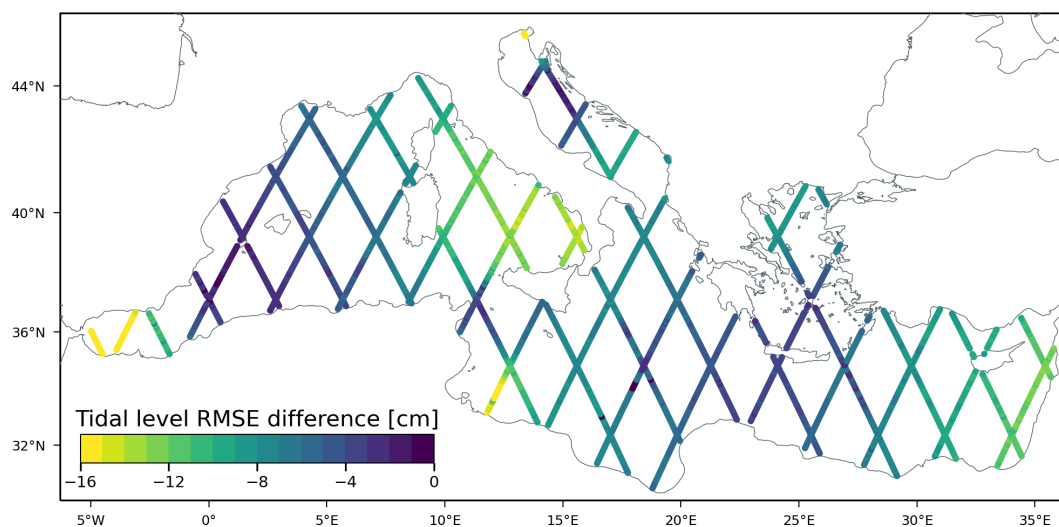

Figure 5. Differences between the CRMSE of the analysis ensemble mean and the CRMSE of the deterministic simulations. The CRMSEs are calculated with respect to the astronomical tide computed by the altimeter X-TRACK along-track tidal constants retrieved from AVISO.

for the 2-month period considered, while for extreme events, the trend is normally the opposite.

In Fig. 8, we report the Taylor diagrams for the total sea level (ZF, ZF_A). In this case, the results are slightly better than for the surge. The simulations, both without and with DA, maintain evident improvements even on the third forecast day. For the total sea level, we can also evaluate the improvement in stations 61 and 62, even if they have a smaller number of records. As seen for the hindcast and reanalysis simulations, these stations are important because of their distance from other assimilated stations and because they are the only stations in the eastern Mediterranean basin. In these two stations, the DA improves the results strongly; this is also the case in the reanalysis simulation.

Figure 9 shows the bias diagram for the total sea level. As for the surge, the biases are positive in most of the stations, denoting a model overestimation, but they are generally lower than those of the surge, even for the model without DA. As shown in the Taylor diagrams, the CRMSEs in Fig. 9 also improve with the DA in all three forecast days, even if more in the first.

3.3.1 12 November 2019's storm surge event

On 12 November 2019, a particularly intense meteorological perturbation hit the central part of the Mediterranean basin. A sub-synoptic cyclone, centred in the Tyrrhenian Sea, caused a strong southeasterly (Sirocco) wind along the entire Adriatic basin, with a fairly typical configuration. However, embed-
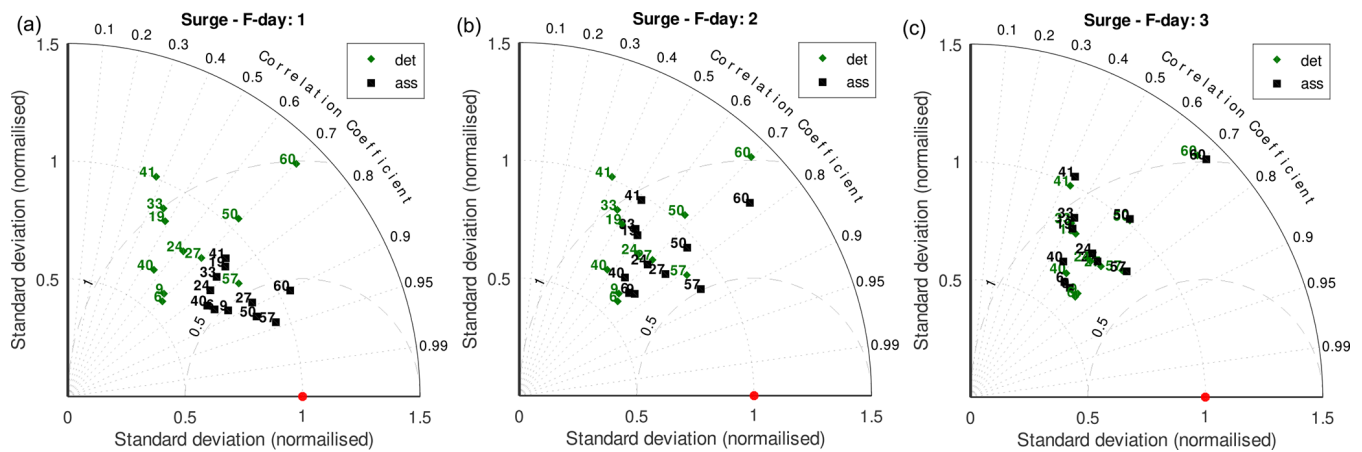
Figure 6. Normalised Taylor diagrams of the forecast simulations with the surge. The deterministic simulations (green diamonds) compared to DA simulations (black squares) for the first- **(a)**, second- **(b)**, and third-day **(c)** forecasts. The red dot indicates the perfect agreement.
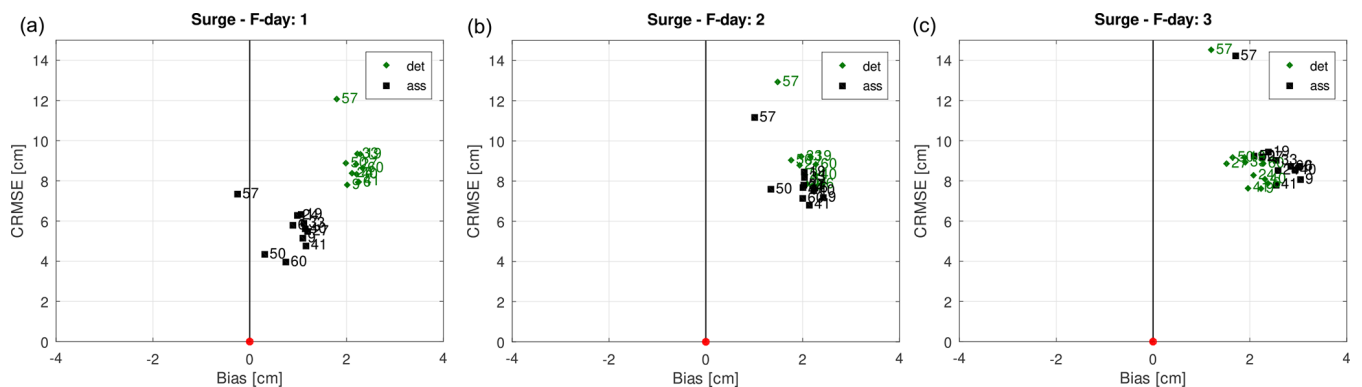

Figure 7. Bias diagrams for the first- **(a)**, the second- **(b)**, and the third-day **(c)** forecasts of the surge simulations. The deterministic results (green diamonds) are plotted with the DA results (black squares). The red dot is the perfect agreement, while positive bias indicates an overestimation by the model.

ded in the first cyclone, a second meso-beta-scale cyclone developed near the southeastern coasts of Italy and moved in the northwestward direction over the Adriatic Sea. This second cyclone moved at a speed close to that of shallow-water waves in the northern Adriatic basin, causing Proudman resonance (Proudman, 1929; Ferrarin et al., 2021). In Venice, the sum of the various sea level contributions produced a maximum which was the second highest ever recorded (Ferrarin et al., 2021).

In Fig. 10, we report the sea level forecast without and with DA the day before the main peak, the day of, and the day after. The sea level is related to the Venice station, and the forecasts are retrieved from the simulations SF and SF_A, with the addition of the tide computed by the harmonic constants. The previous day's atmospheric forecast underestimated the wind and had strong errors in positioning the cyclones. Consequently, the sea level forecast also had large errors (left panel), and the use of the DA had no effect, since the initial state was relative to an instant of calm conditions and

did not contain any large errors. The second forecast, shown in Fig. 10 (central panel), is relative to the day of the event. The meteorological forecast was accurate, with a good reproduction of the track followed by the smaller cyclone. Consequently, the prediction of the sea level is good even without the use of the DA, since, even in this case, the event started to evolve after the time of the initial state. The DA does not improve the main peak, but it corrects slightly the previous peak.

Finally, we show the forecast of the day after because a large peak, even if less extreme than the previous one, was registered in Venice. This event happened with calm weather conditions and was due to an overlap of the tidal peak with a small seiche peak, probably linked to the second mode of the Adriatic basin (A_2 in Table 2). The forecast without DA missed the reproduction of this peak because of errors in the initial state of the surge field in the Adriatic Sea. In this case, the DA was able to contribute valuably, with a correction of about 15 cm, which is considerable (Fig. 10, third panel).
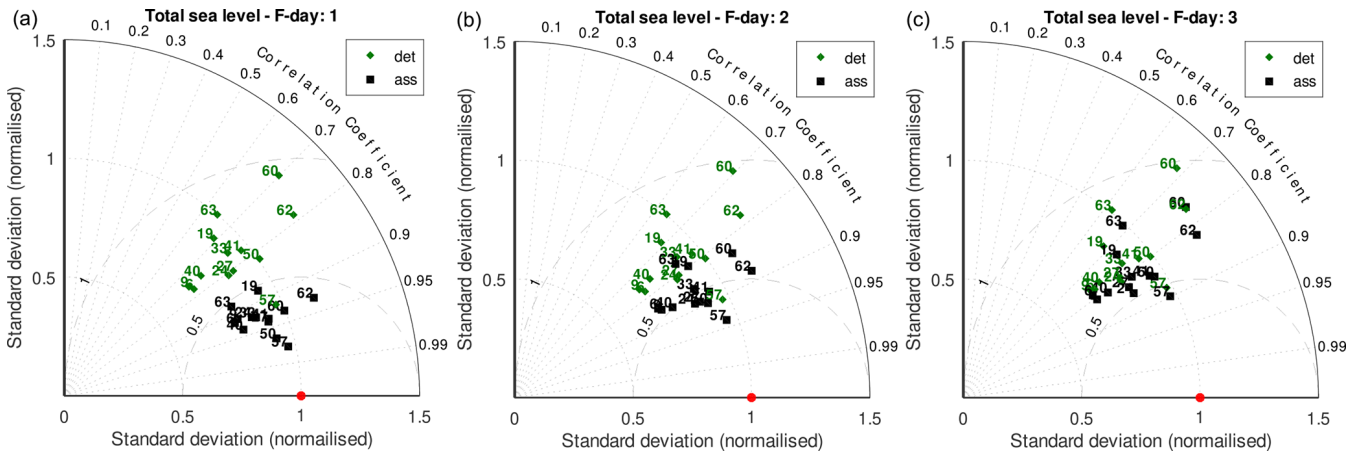
Figure 8. Normalised Taylor diagrams of the forecast simulations with the total sea level. The deterministic simulations (green diamonds) compared to the DA simulations (black squares), for the first- **(a)**, second- **(b)**, and third-day **(c)** forecasts. The red dot is the perfect agreement.
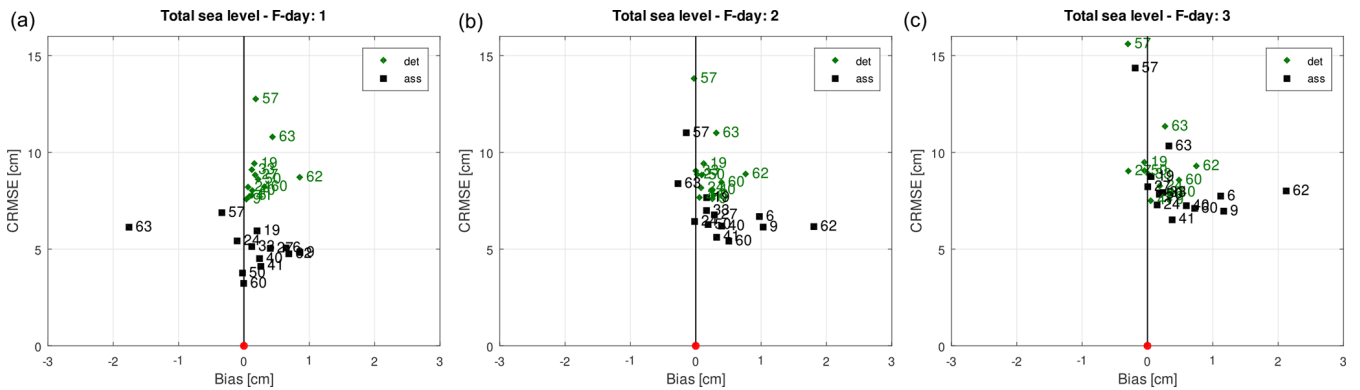

Figure 9. Bias diagrams for the first- **(a)**, second- **(b)**, and third-day **(c)** forecasts of the total sea level simulations. The deterministic results (green diamonds) are plotted with the DA ones (black squares). The red dot is the perfect agreement, while positive bias indicates an overestimation by the model.

3.3.2 December 2019's seiche events

As explained in the introduction, seiches are free barotropic oscillations of the sea level in a basin, triggered by an initial perturbation. Therefore, since they are not forced, the reproduction of their propagation depends solely on a correct initial state and a correct modelling setup. Given that DA has the purpose of reducing the error of the initial state, we expect, as shown in the previous section, a remarkable impact on the reproduction of the seiches.

In December 2019 (period included in our simulations), significant seiche events, among the most energetic ever recorded in this area, took place (Fig. 11). Despite their intensity, they were not preceded by any strong storm surge. A possible explanation could be that these oscillations were triggered by a slightly periodic atmospheric oscillation at a frequency similar to that of the normal modes of the basin (which have the basin's resonant frequencies).

These events were poorly predicted by storm surge models operating at that time in Venice (none with DA), the city most affected by flooding in the northern Adriatic. Figure 12 shows the total sea level recorded at station 56 (Venice) and the first 3 d of forecasting from the surge simulations (SF, SF_A with the addition of the astronomical tide). The oscillations observed in the figure are therefore a superposition of the astronomical tide on the surge signal, which is dominated by the seiche oscillation. At the beginning of the forecast, the DA corrects an error of about 30 cm and maintains a continuous improvement over time, which can also be appreciated after 3 d days of forecasting. Although in Sect. 3.3 we have seen that the statistical improvement after 3 d is not very appreciable, when these oscillations are considerable, the error of the initial state tends to be larger, and the DA provides a greater correction.

To check the spatial patterns of the DA correction in this event, we plotted in Fig. 13 the surge increments of the analysis ensemble mean with respect to the background ensem-

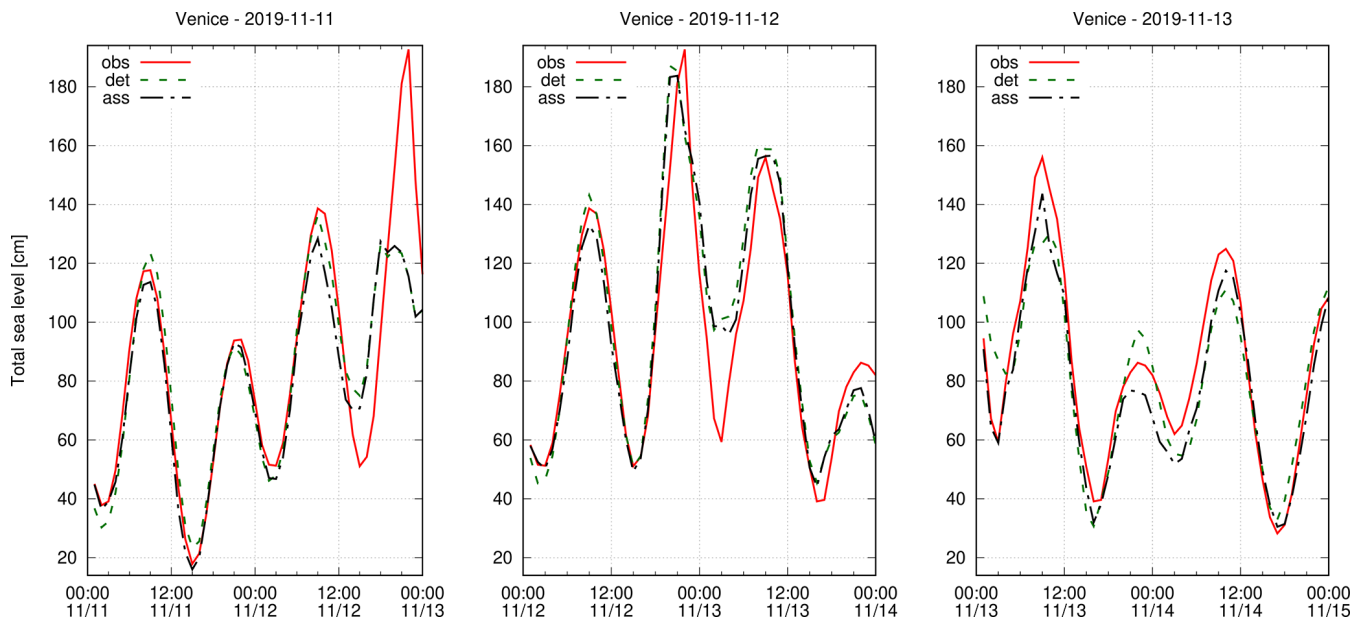**Figure 10.** Forecasts issued on 11, 12, and 13 November 2019 at the Venice station from the surge simulations (adding the tide). The observed total sea level (obs) is compared to the forecast without (det) and with (ass) the use of the DA. The sea levels are in CET time a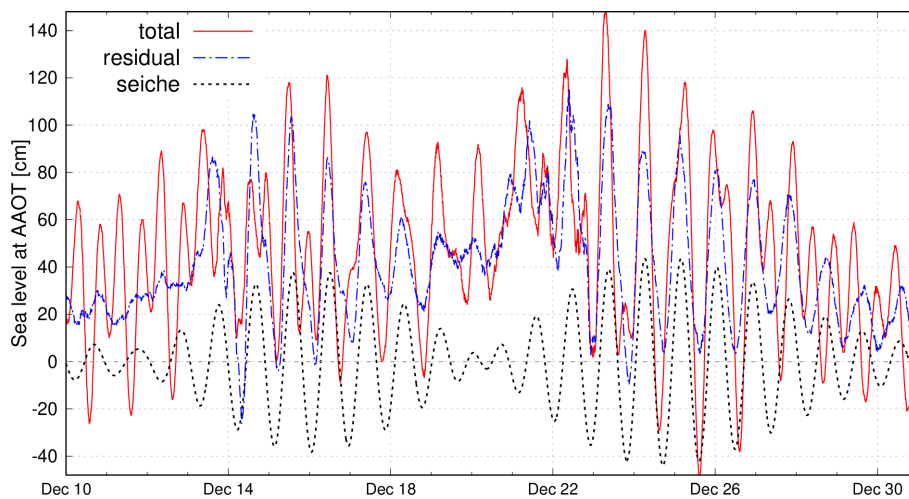nd are referred to the local geodetic reference datum https://www.comune.venezia.it/it/content/riferimenti-altimetrici, last access: 2 May 2023.

Figure 11. The seiche event of December 2019, recorded at the AAOT station (no. 57). From the observed total sea level (total), we extracted the NTR (residual) and the seiche contribution (seiche) with a bandpass filter. The sea levels are in CET time and are referred to the local geodetic reference datum https://www.comune.venezia.it/it/content/riferimenti-altimetrici.

ble mean, averaged over one daily DA cycle, on 14 December 2019. The increments are distributed equally throughout the domain and do not appear to be concentrated in the areas with more stations. This is correct, as variations of barotropic phenomena, which have a very large spatial scale, must be extensive. There could be some wrong increments in the southern and eastern areas, where no stations are assimilated; however, this does not seem to emerge from the statistics of the results, which are also good in this part (e.g. station 60 in Fig. 6 and stations 60, 62, 63 in Fig. 8). Finally, note how

the increments tend towards zero near the open boundary in the Atlantic as a consequence of the Eq. (5) to avoid shocks given by the prescribed sea level.

These events demonstrate the particular effectiveness of the DA in correcting the dynamical state in the presence of seiches. To better highlight this feature, we carried out the spectral analyses of the NTR from the observations and the model surge for all the stations for December 2019. From the peaks in the power spectra, the periods and energy of the excited barotropic modes can be deduced. Before ex-
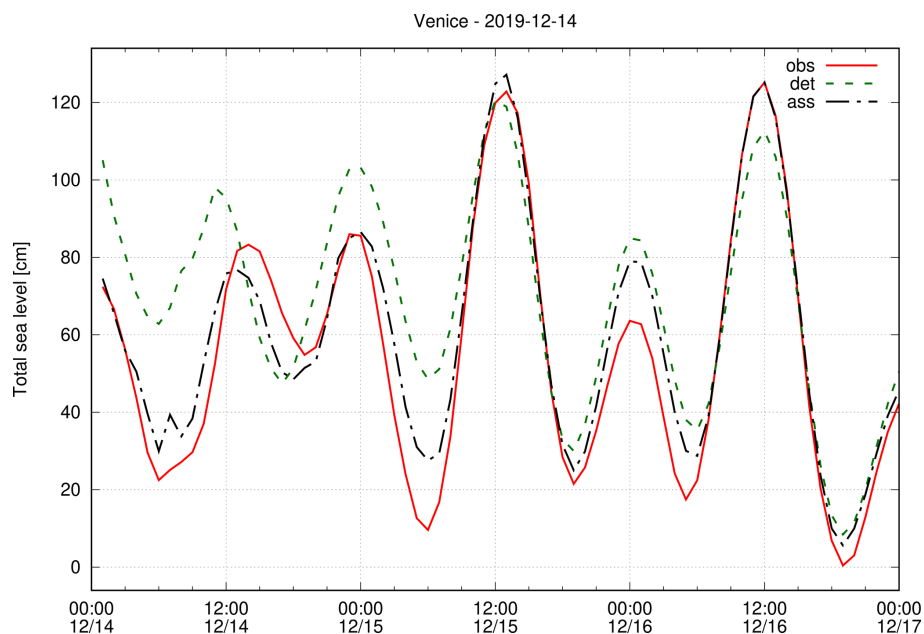
Figure 12. Forecast issued on 14 December 2019 at the Venice station regarding the surge simulations (adding the tide), referred to the local geodetic reference datum https://www.comune.venezia.it/it/content/riferimenti-altimetrici and in CET time. The observed total sea level (obs) compared to the forecast without (det) and with (ass) DA.
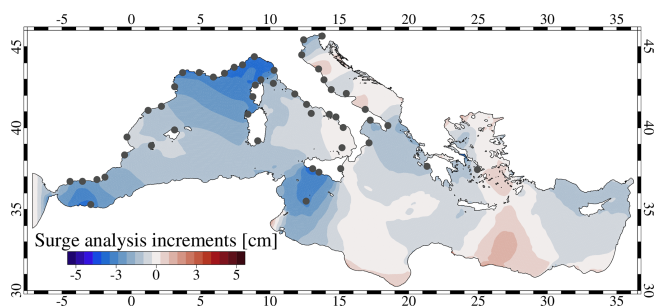

Figure 13. Surge increments of the analysis ensemble mean with respect to the background ensemble mean. The increments are the mean of 24 hourly steps (one daily DA cycle) on 14 December 2019. The assimilated stations are marked as dark-grey dots.

amining the model performances in the reproduction of the power spectra, we give below a summary of the periods of the barotropic modes of the Adriatic and Mediterranean seas. We report the values currently known from works based on observations or models and the periods extracted from our observations (see Table 2). Although the periods of the main modes of the Adriatic Sea are known (Cerovecki et al., 1997; Vilibić et al., 2005; Vilibić, 2006; Bajo et al., 2019), no works based on the analysis of observations (as far as we know) report the periods of the Mediterranean basin. For the Mediterranean Sea, we found only one work that reports the shapes and the periods of the main modes, deduced with a simple model with remarkable accuracy (Schwab and Rao, 1983). In this work, the authors calculated the eigenvalues of a sim-

plified barotropic model of the Mediterranean Sea and found four modes of oscillation. The first mode (M_1) relates to an oscillation with a single positive amphidromic node in the Gulf of Sicily and an expected period of 38.5 h. This mode, which should have a maximum amplitude at both the western and eastern borders of the Mediterranean basin, has not been identified by our observations, probably because it has not been solicited by any forcing in the period that we considered.

The second mode (M_2) has a more complex shape, with a negative amphidromic node in the western basin, a positive one in the eastern basin, and a third one in the Adriatic. This oscillation has an expected period of 11.4 h. A similar peak, with a period of 12.8 h, is present in the power spectra of several stations of the western basin (Fig. 15). The difference from the expected peak can be explained by considering the various simplifications and the low resolution of the model used in Schwab and Rao (1983), which dates back many years.

The third mode (M_3) has three positive amphidromic nodes in the Mediterranean basin and one positive and one negative node in the Adriatic basin. This mode has a period of 8.4 h and a maximum amplitude near the Gibraltar Strait and along the west coast of the Adriatic Sea. Indeed, from our measurements, a peak at 8–8.3 h is quite evident in some stations in the western Mediterranean basin (Fig. 15), and a hinted peak is also present in Trieste (Fig. 14) and in other stations on the western coast of the Adriatic Sea.

Table 2. Periods of the barotropic modes in the Adriatic and Mediterranean basins. A mode identification label is written in the first column. The second column shows the average periods estimated by scientific works by means of observation spectral analysis, the third column shows the periods estimated by the model in Schwab and Rao (1983), and the last column shows our estimation of the periods by means of spectral analysis of the observations.

Mode ID	$T_{ol}[h]$	$T_s[h]$	$T_{op}[h]$
A_1	21.2	20.1	21.3
A_2	10.7	9.3	10.7
A_3	6.7	6.8	–
A_4	5.3	–	5.2
M_1	–	38.5	–
M_2	–	11.4	12.8
M_3	–	8.4	8.3
M_4	–	7.4	–
$M5$	–	–	6.2

Finally, the fourth Mediterranean mode (M_4) of 7.4 h should be related to the main oscillation of the Tunisian bight, where we have no observations, as a result of which we cannot check its presence. From the observation power spectra that we have analysed, there seems to exist a fifth mode that we called M_5, visible in the stations of the western Mediterranean basin and with a period of 6.2 h (Fig. 15). However, to our knowledge, there is no information about this oscillation in the scientific literature.

Regarding the Adriatic Sea, the fundamental mode, here referred to as A_1, is an oscillation that covers the entire basin, with a nodal line south of the Strait of Otranto, near the 1000 m bathymetric line, and a period of about 21.2 h. This oscillation is the most energetic among those analysed and is clearly visible in the observation power spectra, with a period of 21.3 h (Fig. 14).

The second Adriatic mode (A_2) has a nodal line that cuts the basin north of Ancona and a second line south of the nodal line of the fundamental mode, near the 2000 m bathymetric line. This oscillation is quite energetic, albeit less so than the main one, and has a period of about 10.7 h, which is perfectly confirmed by our observations (Fig. 14). Finally, the third Adriatic mode (A_3) has a nodal line under the Po delta, one just above the Gargano peninsula, and a third line coinciding with that of the fundamental mode. This oscillation has a period of about 6.7 h, but we did not detect it in our power spectra. It is probable that even this mode was not triggered during the 2-month period that we analysed.

Finally, in Trieste and in other Adriatic stations, there is a peak at 5.2 h, which we called A_4. This peak cannot be the Trieste bay seiche, which has a period of 2.7–4.2 h (Šepić et al., 2022), and was also found by Šepić et al. (2022), with a value of 5.3 h. Its origin is still unclear.

After this description of the barotropic modes of the Mediterranean and the Adriatic basins, we show now how the model reproduces them on the first day of the forecast simulations (SF, SF_A). Figure 14 shows the power spectra for two stations in the Adriatic Sea: Trieste in the northern part and Bari near the end of the basin in the southern part. Both the peaks of the fundamental mode, A_1, and that of the second mode, A_2, are clearly visible in these stations. Note that the peaks are much more energetic in Trieste than in Bari, which is located near the nodal lines of the two modes. The two peaks are both underestimated by the model without DA, while with the DA, the peak of the first mode is reproduced very well, especially in the north. The A_2 peak remains slightly underestimated at both stations but improves significantly with respect to the simulation without DA. Finally, at the Trieste station, a peak corresponding to the period of the third mode of the Mediterranean Sea (M_3) is slightly visible in the observations. However, the model power spectra, both with and without DA, are noisy in this part of the frequencies and do not reproduce this peak. Still, in Fig. 14, but only at the Trieste station, the A_4 peak is well visible in the observation power spectrum, but it is not reproduced by the model. This peak could be related to some local atmospheric phenomenon not present in our forcing.

In Fig. 15, we show the power spectra of two stations near Gibraltar, one on the European coast and one on the African coast. In both stations, the second and third barotropic modes of the Mediterranean basin are well visible (M_2, M_3). Their energy is much lower than that of the Adriatic modes (about 1000 times lower), and, probably for this reason, they are corrected less by the DA. Both stations and many others in the western Mediterranean basin show a third, more energetic peak, which could be a fifth barotropic mode (M_5). We can exclude the possibility that this peak is a spurious signal from a partial subtraction of the astronomical tide from the NTR, as it is also present in the surge signal of the model without DA (SF). This peak is corrected by the DA even though it is broadened in frequency.

4 Discussion

Looking at the results just presented, we can state that DA has an overall positive impact on the reproduction of barotropic sea level signals in the Mediterranean Sea. In the case of the astronomical tide, more than for the other components, the DA has shown that it can provide an excellent correction of the simulated sea level, even in areas very far from the assimilated stations. This fact has been confirmed in both the areas with few stations, such as the eastern Mediterranean, and in the open sea. In fact, although the assimilated stations are all coastal, the altimetric data allowed the tidal results in the open sea to be validated. The effectiveness of DA is due to the good number of ensemble members and the good quality of the perturbations. It is probable that, when using localisation techniques, the improvement would be weaker, since these techniques limit the correction to areas much closer to
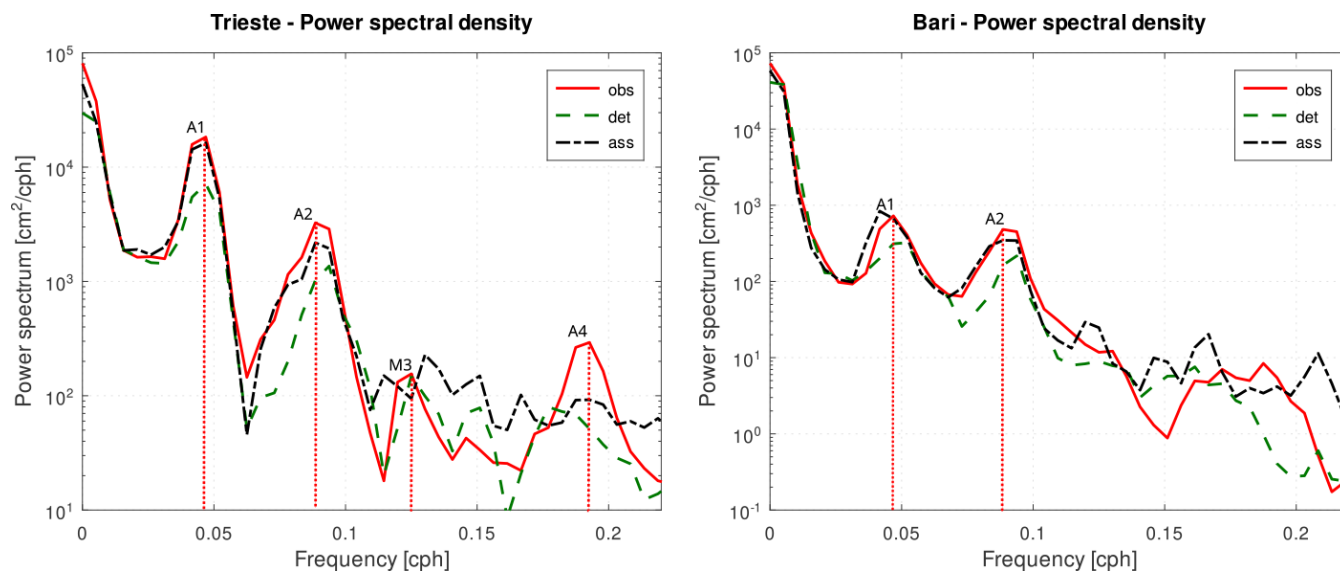
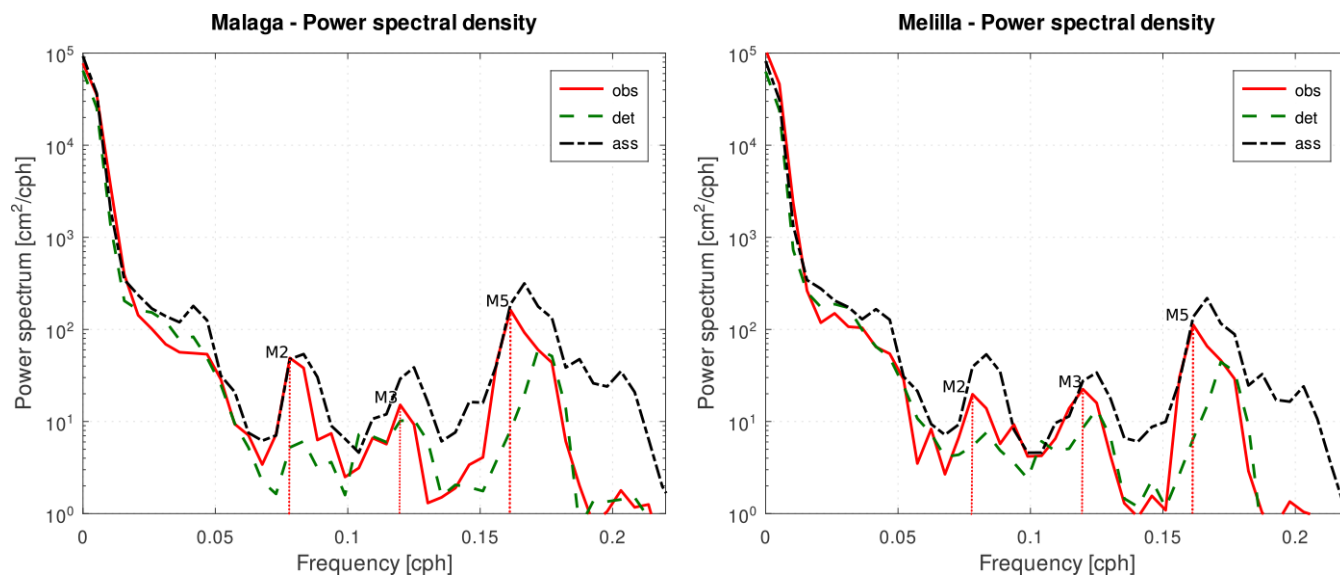**Figure 14.** Power spectral density of the sea level in Trieste and Bari in the Adriatic Sea.

Figure 15. Power spectral density of the sea level in Málaga and Melilla in the western Mediterranean Sea.

the assimilated stations. Without localisation, the analysis increments extend to the entire computational grid (Fig. 13). Furthermore, from a physical point of view, the astronomical tide and the other barotropic components have large characteristic spatial lengths which translate into sea level correlations at large distances and into greater spatial effectiveness of the DA. What makes astronomical tide different from surge and seiches is its periodicity and being referred to as a mean sea level perfectly constant in time. This avoids any bias in the departures of the assimilation, which are more difficult to deal with than the surge and total sea level. These two facts probably contribute to making the astronomical tide results better than those for the other sea level components.

On the contrary, the surge component is not periodic at all, and its error mainly depends on the errors in the atmospheric forcings. In the case of the Mediterranean Sea, which is surrounded by a complex orography and is often subject to complex meteorological situations, the atmospheric models can have large errors due to the lack of resolution, unresolved processes (hydrostatic models), and the lack of high-resolution DA. Their errors result in errors in the surge component which cannot be corrected by the DA in the ocean model when making forecasts. However, in the reanalysis simulation, if the assimilation step is short enough (e.g. hourly), the dynamical system is strongly driven by DA, and the error coming from the forcing cannot grow too much.

In the forecast simulations, the DA impact is due to the reduction of the error of the initial state. The error of the initial state propagates over time and sums up the atmospheric forcing error. Analysing the results statistically, the simulations without DA do not show much deterioration from the first to the third forecast day. However, this is not true in the case of extreme events, when meteorological forcing generally has a larger error. In these cases, even the error of the initial state is often larger due to pre-existing seiches deriving from previous storms. This error can be corrected by DA, and the improvement extends over several days, depending on the energy and the damping time of the seiche oscillations. The DA improves the error not only of the seiche part but also of other sea level components, such as of the tidal part (in the total sea level forecast) or of surge phenomena growing at the time of the analysis. However, in order to catch the formation of a surge in an operational context, the EnKF should be executed with hourly updates. With one or two updates per day, DA is still a valuable tool for correcting the seiche and the tidal parts.

Regarding the computational cost, although there is a need to use a significant number of ensemble members, this is rather low. The ensemble member simulations are perfectly parallel and can run independently between each analysis step. Moreover, barotropic simulations are fast, as the equations are quite simple, and there is no need to simulate the advection and/or diffusion of temperature and salinity. Our workstation is a single-blade mid-level server, with 96 cores and the 81 ensemble members run in parallel. The generation of the ensemble forcings and boundary conditions takes about 5 min, after which the ensemble simulations run parallel, except in the 24 analysis steps, where the code is parallelised as well. The total time for carrying out the entire assimilation procedure is approximately 25 min, of which approximately 5 min are necessary to carry out 5 d of forecasting.

Finally, we dedicated the last part to the study of the seiches. In the forecast, we have seen that the DA can lead to a significant improvement, especially where these oscillations are very energetic, as in the Adriatic Sea. As previously mentioned, while in the Adriatic Sea oscillations' characteristics are more studied, with the exception of the oscillation A_4, which has an unclear origin, they have not been analysed much in the Mediterranean Sea. The observations in our possession confirm and partially correct the periods found in Schwab and Rao (1983) as far as the M_2 and M_3 modes are concerned. However, we did not detect the period of the main mode of the Mediterranean Sea, probably because it has not been triggered in the 2 months that we have analysed, but further investigation is needed. Then we detected a Mediterranean barotropic oscillation with a period of 6.2 h, which we called M5, but it is not present in the literature even if its peak is evident in many validation (shown) and calibration (not shown) stations along the coasts of the western Mediterranean basin. This oscillation, which is more energetic than

M_2 and M_3, is underestimated by the model without DA, and even with the use of DA, it is not reproduced correctly. Considering that oscillations with a longer period are reproduced better, even if they are less energetic, it is possible that the DA has more difficulty in correcting the high-frequency oscillations. This may be due to the hourly time step between the observations, which may be too long to resolve these modes.

5 Conclusions

In this paper, we investigated the impact of DA in reproducing the barotropic components of the sea level in the Mediterranean Sea. We analysed the performances of the model without and with DA in hindcast and reanalysis simulations and in forecast simulations starting from an initial hindcast or analysis state. The barotropic components of the sea level that we considered are the astronomical tide, the surge, the associated seiches, and the total sea level given by their sum. The results show very good performance of the DA in reanalysis, with the error in the tide reproduction reduced by a third on average, and slightly worse performances, but always more than good, for the surge and the total sea level. In the case of the surge and the total sea level, the DA corrects them even in the presence of large errors in the atmospheric forcing thanks to a sufficiently high assimilation frequency (1 h), a good number of ensemble members, and a sufficient number of assimilated observations. The improvements made by the DA in the forecast depend on the reduction of the error of the initial state, but the error coming from the atmospheric forcing (and lateral boundary conditions) cannot be reduced. However, the DA still has a positive impact, especially on the first-day forecast, gradually decreasing over the following days until the simulations' performances without DA were reached. The improvement can last longer when seiche oscillations are present. In this case, the initial correction propagates in the following days with a period and decay time equal to those of the triggered barotropic mode. Finally, still considering the forecast simulations, the bias error is lower in the total sea level simulations than in the surge ones.

In the last part of the results, we have analysed the periods of the barotropic modes of the Adriatic and Mediterranean basins, obtained by means of the observation power spectra and reproduced by the model. In the Adriatic, we detected the periods of the two main modes (A_1, A_2), a fourth mode not well known (A_4), and the third Mediterranean mode (M_3). In the Mediterranean basin, outside the Adriatic, we detected the periods of the second and third modes (M_2, M_3) and of a mode that we called M_5 (6.2 h). We tested the reproduction of the associated power peaks by the model in the first-day forecast. While the periods are also well reproduced without DA, the energy of the spectral peaks improves with DA, thus confirming the better reproduction of these oscillations. We also noticed that the DA improves the low-

frequency modes more, while it has some difficulties with high-frequency modes. This is probably due to the sampling rate of 1 h, which is not high enough.

This work provides a preliminary test of the use of the DA for the reanalysis of tides, surges, and seiches in the Mediterranean Sea. Reanalysis simulations can be extended to several years for climatological studies, obtaining good performances, as the DA is able to overcome deficiencies in the atmospheric forcing and boundary conditions. Further improvements for the reanalysis, where the error must be low during the whole simulation period, can be obtained using an ensemble Kalman smoother (EnKS). The EnKS is easily applicable to simulations with the EnKF if localisation techniques are not used. With regards to DA methodologies, an improvement for the reanalysis, as well as for the forecast, would be the use of parameter estimation techniques, such as using an augmented state in the EnKF (Evensen, 2009b). The parameter estimation allows some model parameters to be calibrated, typically the drag coefficient at the bottom. This method could reduce the model error, but then also, the DA in its traditional form should be used in order to reduce the error of the initial state. Finally, increasing the number of the assimilated observations from in situ stations and altimeters would lead to a further improvement, especially if these are available in areas not well covered. However, while the use of in situ data is quite easy, as discussed before, the altimetric data are difficult to use in storm surge applications (Bajo et al., 2017), and further investigations are needed.

With regards to the barotropic modes in the Mediterranean and Adriatic basins, some of them are not well understood, and their shapes, periods, and decay times should be determined with more precision. In this context, DA can be used to provide a reliable reanalysis of the surge from which to extract the seiche part.

The model and the DA system tested in this work will be used, with a similar configuration, in an operational system for forecasting the sea level in several locations of the Mediterranean coasts, with a focus on the Italian coasts. The system will be installed at the ISPRA Centre and will retrieve the observations from the stations along the Italian coast, providing a 5 d forecast.

Appendix A: In situ coastal stations

In this Appendix, we present a table with the in situ stations, their identification numbers, and their positions. We used these stations in the paper for the data assimilation and as validation stations.

Table A1. List of stations with sea level measurements. The stations with an asterisk are those used in the validation, while the others have been assimilated. The numbering is the one used in the paper, and the stations' geographical coordinates are reported as well.

ID	Long	Lat	Station	ID	Long	Lat	Station
1	−2.930	35.290	Melilla	35	14.750	40.676	Salerno
2	−4.417	36.711	Málaga	36	15.275	40.029	Palinuro
3	−3.520	36.720	Motril	37	15.190	38.785	Ginostra
4	−2.478	36.830	Almeria	38	8.403	40.842	Porto-Torres
5	−1.899	36.974	Carboneras	39	9.114	39.210	Cagliari
6*	−0.973	37.596	Murcia	40*	8.309	39.147	Carloforte
7	−0.481	38.338	Alicante	41*	13.371	38.121	Palermo
8	−0.310	39.440	Valencia	42	13.076	37.504	Sciacca
9*	1.419	38.734	Formentera	43	13.526	37.285	Porto-Empedocle
10	1.450	38.917	Ibiza	44	15.093	37.498	Catania
11	3.117	39.867	Alcúdia	45	12.604	35.499	Lampedusa
12	1.213	41.078	Tarragona	46	17.137	39.083	Crotone
13	2.160	41.340	Barcelona	47	17.223	40.475	Taranto
14	3.107	42.520	Port-Vendres	48	18.497	40.147	Otranto
15	3.699	43.397	Sète	49	16.866	41.140	Bari
16	4.893	43.405	Fos-sur-Mer	50*	16.177	41.888	Vieste
17	5.914	43.122	Toulon	51	15.501	42.119	Tremiti
18	6.717	43.359	Port Ferréol	52	14.414	42.355	Ortona
19*	6.933	43.483	La Figueirette	53	13.890	42.960	San Benedetto del Tronto
20	7.421	43.728	Monaco	54	13.506	43.624	Ancona
21	9.350	42.967	Centuri	55	12.282	44.492	Ravenna
22	8.938	42.635	L'Île-Rousse	56	12.426	45.418	Venice
23	8.760	41.920	Ajaccio	57*	12.511	45.313	AAOT
24*	9.374	41.836	Solenzara	58	13.757	45.649	Trieste
25	8.018	43.878	Imperia	59	21.319	37.640	Katakolo
26	8.870	44.380	Genova	60*	23.621	37.935	Peiraias
27*	9.857	44.096	La-Spezia	61	24.941	37.438	Syros
28	10.299	43.546	Livorno	62*	35.653	34.242	Batroun
29	10.238	42.742	Marina-di-Campo	63*	29.879	31.209	Alexandria
30	11.789	42.093	Civitavecchia				
31	12.634	41.446	Anzio				
32	12.965	40.895	Ponza				
33*	13.589	41.209	Gaeta				
34	14.269	40.841	Napoli				

References

Bajo, M.: Improving storm surge forecast in Venice with a unidimensional Kalman filter, Estuar. Coast. Shelf Sci., 239, 106773, https://doi.org/10.1016/j.ecss.2020.106773, 2020.

Bajo, M.: SHYFEM model with EnKF, Zenodo [code], https://doi.org/10.5281/zenodo.7886239, 2023.

Bajo, M. and Umgiesser, G.: Storm surge forecast through a combination of dynamic and neural network models, Ocean Model., 33, 1–9, https://doi.org/10.1016/j.ocemod.2009.12.007, 2010.

Bajo, M., Zampato, L., Umgiesser, G., Cucco, A., and Canestrelli, P.: A finite element operational model for storm surge prediction in Venice, Estuar. Coast. Shelf Sci., 75, 236–249, https://doi.org/10.1016/j.ecss.2007.02.025, 2007.

Bajo, M., Biasio, F. D., Umgiesser, G., Vignudelli, S., and Zecchetto, S.: Impact of using scatterometer and altimeter data on storm surge forecasting, Ocean Model., 113, 85–94, https://doi.org/10.1016/j.ocemod.2017.03.014, 2017.

Bajo, M., Međugorac, I., Umgiesser, G., and Orlić, M.: Storm surge and seiche modelling in the Adriatic Sea and the impact of data assimilation, Q. J. Roy. Meteor. Soc., 145, 2070–2084, https://doi.org/10.1002/qj.3544, 2019.

Barbariol, F., Pezzutto, P., Davison, S., Bertotti, L., Cavaleri, L., Papa, A., Favaro, M., Sambo, E., and Benetazzo, A.: Wind-wave forecasting in enclosed basins using statistically downscaled global wind forcing, Front. Mar. Sci., 9, 1002786, https://doi.org/10.3389/fmars.2022.1002786, 2022.

Bertin, X., Li, K., Roland, A., Zhang, Y. J., Breilh, J. F., and Chaumillon, E.: A modeling-based analysis of the flooding associated with Xynthia, central Bay of Biscay, Coast. Engin., 94, 80–89, https://doi.org/10.1016/j.coastaleng.2014.08.013, 2014.

Birol, F., Fuller, N., Lyard, F., Cancet, M., Niño, F., Delebecque, C., Fleury, S., Toublanc, F., Melet, A., Saraceno, M., and Léger, F.: Coastal applications from nadir altimetry: Example of the X-TRACK regional products, Adv. Space Res., 59, 936–953, https://doi.org/10.1016/j.asr.2016.11.005, 2017.

Byrne, D., Horsburgh, K., and Williams, J.: Variational data assimilation of sea surface height into a regional storm surge model: Benefits and limitations, J. Oper. Oceanogr., 16, 1–14, https://doi.org/10.1080/1755876X.2021.1884405, 2021.

Carrassi, A., Bocquet, M., Bertino, L., and Evensen, G.: Data assimilation in the geosciences: An overview of methods, issues, and perspectives, Wiley Interdisciplinary Reviews, Climate Change, 9, e535, https://doi.org/10.1002/wcc.535, 2018.

Carrère, L. and Lyard, F.: Modeling the barotropic response of the global ocean to atmospheric wind and pressure forcing – comparisons with observations, Geophys. Res. Lett., 30, 1275, https://doi.org/10.1029/2002GL016473, 2003.

Cavaleri, L., Bajo, M., Barbariol, F., Bastianini, M., Benetazzo, A., Bertotti, L., Chiggiato, J., Davolio, S., Ferrarin, C., Magnusson, L., Papa, A., Pezzutto, P., Pomaro, A., and Umgiesser, G.: The October 29, 2018 storm in Northern Italy – An exceptional event and its modeling, Prog. Oceanogr., 178, 102178, https://doi.org/10.1016/j.pocean.2019.102178, 2019.

Cerovecki, I., Orlić, M., and Hendershott, M. C.: Adriatic seiche decay and energy loss to the Mediterranean, Deep-Sea Res. Pt. I, 44, 2007–2029, https://doi.org/10.1016/S0967-0637(97)00056-3, 1997.

Clementi, E., Aydogdu, A., Goglio, A., Pistoia, J., Escudier, R., Drudi, M., Grandi, A., Mariani, A., Lyubartsev, V., Lecci, R., Cretí, S., Coppini, G., Masina, S., and Pinardi, N.: Mediterranean Sea Physical Analysis and Forecast (CMEMS MED-Currents, EAS6 system) (Version 1), https://doi.org/10.25423/CMCC/, 2021.

Evensen, G.: Sequential data assimilation with a nonlinear quasi-geostrophic model using Monte Carlo methods to forecast error statistics, J. Geogr. Res., 99, 10143–10162, 1994.

Evensen, G.: The Ensemble Kalman Filter: theoretical formulation and practical implementation, Ocean Dynam., 53, 343–367, https://doi.org/10.1007/s10236-003-0036-9, 2003.

Evensen, G.: Sampling strategies and square root analysis schemes for the EnKF, Ocean Dynam., 54, 539–560, https://doi.org/10.1007/s10236-004-0099-2, 2004.

Evensen, G.: Spurious correlations, localization, and inflation, Springer Berlin Heidelberg, Berlin, Heidelberg, 237–253, https://doi.org/10.1007/978-3-642-03711-5_15, 2009a.

Evensen, G.: The ensemble Kalman filter for combined state and parameter estimation, IEEE Control Syst. Mag., 29, 83–104, https://doi.org/10.1109/MCS.2009.932223, 2009b.

Fernández-Montblanc, T., Vousdoukas, M., Ciavola, P., Voukouvalas, E., Mentaschi, L., Breyiannis, G., Feyen, L., and Salamon, P.: Towards robust pan-European storm surge forecasting, Ocean Model., 133, 129–144, https://doi.org/10.1016/j.ocemod.2018.12.001, 2019.

Ferrarin, C., Roland, A., Bajo, M., Umgiesser, G., Cucco, A., Davolio, S., Buzzi, A., Malguzzi, P., and Drofa, O.: Tide-surge-wave modelling and forecasting in the Mediterranean Sea with focus on the Italian coast, Ocean Model., 61, 38–48, https://doi.org/10.1016/j.ocemod.2012.10.003, 2013.

Ferrarin, C., Bellafiore, D., Sannino, G., Bajo, M., and Umgiesser, G.: Tidal dynamics in the inter-connected Mediterranean, Marmara, Black and Azov seas, Prog. Oceanogr., 161, 102–115, https://doi.org/10.1016/j.pocean.2018.02.006, 2018.

Ferrarin, C., Bajo, M., Benetazzo, A., Cavaleri, L., Chiggiato, J., Davison, S., Davolio, S., Lionello, P., Orlić, M., and Umgiesser, G.: Local and large-scale controls of the exceptional Venice floods of November 2019, Prog. Oceanogr., 197, 102628, https://doi.org/10.1016/j.pocean.2021.102628, 2021.

Flowerdew, J., Horsburgh, K., Wilson, C., and Mylne, K.: Development and evaluation of an ensemble forecasting system for coastal storm surges, Q. J. Roy. Meteor. Soc., 136, 1444–1456, https://doi.org/10.1002/qj.648, 2010.

Gaspari, G. and Cohn, S. E.: Construction of correlation functions in two and three dimensions, Q. J. Roy. Meteor. Soc., 125, 723–757, https://doi.org/10.1002/qj.49712555417, 1999.

Hersbach, H.: Sea Surface Roughness and Drag Coefficient as Functions of Neutral Wind Speed, J. Phys. Oceanogr., 41, 247–251, https://doi.org/10.1175/2010JPO4567.1, 2011.

Horsburgh, K., Haigh, I., Williams, J., De Dominicis, M., Wolf, J., Inayatillah, A., and Byrne, D.: "Grey swan" storm surges pose a greater coastal flood hazard than climate change, Ocean Dynam., 71, 715–730, https://doi.org/10.1007/s10236-021-01453-0, 2021.

Järvinen, H. and Undén, P.: Observation screening and background quality control in the ECMWF 3D-Var data assimilation system, ECMWF Technical Memoranda, 236, 33 pp., https://doi.org/10.21957/lyd3q81, 1997.

Kalnay, E.: Atmospheric Modeling, Data Assimilation and Predictability, Cambridge University Press, https://doi.org/10.1017/CBO9780511802270, 2002.

Kepert, J. D.: On ensemble representation of the observation-error covariance in the Ensemble Kalman Filter, Ocean Dynam., 54, 561–569, https://doi.org/10.1007/s10236-004-0104-9, 2004.

Lyard, F. H., Allain, D. J., Cancet, M., Carrère, L., and Picot, N.: FES2014 global ocean tide atlas: design and performance, Ocean Sci., 17, 615–649, https://doi.org/10.5194/os-17-615-2021, 2021.

Mariani, S., Casaioli, M., Coraci, E., and Malguzzi, P.: A new high-resolution BOLAM-MOLOCH suite for the SIMM forecasting system: assessment over two HyMeX intense observation periods, Nat. Hazards Earth Syst. Sci., 15, 1–24, https://doi.org/10.5194/nhess-15-1-2015, 2015.

Međugorac, I., Pasarić, M., Pasarić, Z., and Orlić, M.: Two recent storm-surge episodes in the Adriatic, Int. J. Safet. Secur. Eng., 6, 589 – 596, https://doi.org/10.2495/SAFE-V6-N3-589-596, 2016.

Pérez, B., Fanjul, E. A., Pérez, S., De Alfonso, M., and Vela, J.: Use of tide gauge data in operational oceanography and sea level hazard warning systems, J. Operat. Oceanogr., 6, 1–18, https://doi.org/10.1080/1755876X.2013.11020147, 2013.

Proudman, J.: The Effects on the Sea of Changes in Atmospheric Pressure, Geophys. J. Int., 2, 197–209, https://doi.org/10.1111/j.1365-246X.1929.tb05408.x, 1929.

Pugh, D. T.: Tides, surges and mean sea-level (reprinted with corrections), Chichester, UK. John Wiley & Sons, Ltd., 486 pp., ISBN: 047191505X, 1996.

Roland, A., Cucco, A., Ferrarin, C., Hsu, T.-W., Liau, J.-M., Ou, S.-H., Umgiesser, G., and Zanke, U.: On the development and verification of a 2-D coupled wave-current model on unstructured meshes, J. Mar. Syst., 78, S244–S254, https://doi.org/10.1016/j.jmarsys.2009.01.026, 2009.

Sakov, P., Counillon, F., Bertino, L., Lisæter, K. A., Oke, P. R., and Korablev, A.: TOPAZ4: an ocean-sea ice data assimilation system for the North Atlantic and Arctic, Ocean Sci., 8, 633–656, https://doi.org/10.5194/os-8-633-2012, 2012.

Schwab, D. and Rao, D.: Barotropic oscillations of the Mediterranean and Adriatic seas, Tellus A, 35, 417–427, 1983.

Scicchitano, G., Scardino, G., Monaco, C., Piscitelli, A., Milella, M., De Giosa, F., and Mastronuzzi, G.: Comparing impact effects of common storms and Medicanes along the coast of south-eastern Sicily, Mar. Geol., 439, 106556, https://doi.org/10.1016/j.margeo.2021.106556, 2021.

Smagorinsky, J.: General circulation experiments with the primitive equations: I. the basic experiment, Mon. Weather Rev., 91, 99–164, https://doi.org/10.1175/1520-0493(1963)091<0099:GCEWTP>2.3.CO;2, 1963.

Storto, A.: Variational quality control of hydrographic profile data with non-Gaussian errors for global ocean variational data assimilation systems, Ocean Model., 104, 226–241, https://doi.org/10.1016/j.ocemod.2016.06.011, 2016.

Taylor, K. E.: Summarizing multiple aspects of model performance in a single diagram, J. Geophys. Res.-Atmos., 106, 7183–7192, https://doi.org/10.1029/2000JD900719, 2001.

Tsimplis, M. N., Proctor, R., and Flather, R. A.: A two-dimensional tidal model for the Mediterranean Sea, J. Geophys. Res.-Ocean., 100, 16223–16239, https://doi.org/10.1029/95JC01671, 1995.

Umgiesser, G., Melaku Canu, D., Cucco, A., and Solidoro, C.: A finite element model for the Venice Lagoon, Development, set up, calibration and validation, J. Mar. Syst., 51, 123–145, ISSN 0924-7963, doi10.1016/j.jmarsys.2004.05.009, 2004.

Vilibić, I.: The role of the fundamental seiche in the Adriatic coastal floods, Cont. Shelf Res., 26, 206–216, https://doi.org/10.1016/j.csr.2005.11.001, 2006.

Vilibić, I., Domijan, N., and Cupic, S.: Wind versus air pressure seiche triggering in the Middle Adriatic coastal waters, J. Mar. Syst., 57, 189–200, https://doi.org/10.1016/j.jmarsys.2005.04.007, 2005.

Šepić, J., Pasarić, M., Međugorac, I., Vilibić, I., Karlović, M., and Mlinar, M.: Climatology and process-oriented analysis of

the Adriatic sea level extremes, Prog. Oceanogr., 209, 102908, https://doi.org/10.1016/j.pocean.2022.102908, 2022.

Welch, P.: The use of fast Fourier transform for the estimation of power spectra: A method based on time averaging over short, modified periodograms, IEEE T. Audio Speech., 15, 70–73, https://doi.org/10.1109/TAU.1967.1161901, 1967.